Available online at www.sciencedirect.com
SCIENCE DIRECT
Polymer 46 (2005) 1583–1594
polymer
www.elsevier.com/locate/polymer

Investigation of the electronic structure and spectroelectrochemical properties of conductive polymer nanotube arrays

L. Dauginet-De Pra, S. Demoustier-Champagne*[1]

Université Catholique de Louvain, Unité de Chimie et de Physique des Hauts Polymères, Croix du Sud, 1. B-1348 Louvain-la-Neuve, Belgium

Received 23 July 2004; received in revised form 17 November 2004; accepted 7 December 2004
Available online 12 January 2005

Abstract

New nanoporous polymeric templates supported on conductive substrates (gold-coated Si wafers or ITO-glass) were used to electrosynthesize polypyrrole (PPy) nanotube brushes. The influence of different synthesis conditions (template pore size, electrodeposition potential and temperature) on the resulting structure and properties of the nanotubes were investigated. X-ray photoelectron, Raman and UV–Vis–NIR spectroscopies were used to characterize the doping level, the conjugation length, and the electronic structure of PPy nanotubes. For the first time, we also report on the redox properties of PPy nanotubes using in-situ UV–Vis spectroelectrochemistry.

Keywords: Polypyrrole nanotube brushes; Supported templates; Electronic structure

1. Introduction

Nanomaterials constitute an emerging subdiscipline of the chemical and materials science that deals with the development of methods for synthesizing nanoscopic particles of a desired material and with scientific investigations of the nanomaterial obtained. The current interest in nanoscale structures comes from their expected unique physical (e.g. electronic, optical, magnetic, mechanical) properties on account of their finite small size and also from their potential wide-ranging implications to a variety of areas, including chemistry, physics, electronics, optics, materials science and biomedical sciences. In particular, the synthesis and characterization of molecular conductors is nowadays a field of intensive research. Therefore, the control of the morphology of conductive polymers is a very stimulating challenge, the production of molecular wires and tubules being a very actively pursued target.

Among the different strategies reported in the literature [1] to synthesize nanostructures, template synthesis is an elegant approach. Martin and his coworkers [2] were the first exploring a method called 'template synthesis' for the preparation of a variety of micro- and nanofibres. This process involves synthesizing the desired material within the void spaces of a porous host material. To date most of the work in template synthesis deal with the use of 'track-etched' polymeric membranes as templates for the chemical or electrochemical synthesis of various metallic or conductive polymer nanowires and nanotubes [2–14]. The most studied systems based on conductive polymers are polypyrrole (PPy) and polyaniline (PANi) nanotubes [3,14]. For small pore diameters, the electrical [5,6,12–15] properties of the conducting polymer nanotubes were found to be largely enhanced relative to more conventional forms of the polymer.

Recently, a new generation of track-etched templates, constituted of nanoporous thin polycarbonate (PC) films supported on various substrates (ITO glass or gold-coated Si wafers) was developed in our lab [16]. The thickness of these supported templates can be varied between 200 nm and several μm and the pore diameter between 15 and 100 nm. The track-etching process consists in an irradiation of the polymer layer by energetic heavy ions creating linear damage tracks, followed by a light sensitization and a

* Corresponding author. Tel.: +32 10 473560; fax: +0032 10 451593.
E-mail address: demoustier@poly.ucl.ac.be (S. Demoustier-Champagne).
[1] Research Associate of the Belgium National Funds for Scientific Research (F.N.R.S.).

0032-3861/$ - see front matter © 2004 Elsevier Ltd. All rights reserved.
doi:10.1016/j.polymer.2004.12.016

chemical etching of these tracks to cylindrical pores. From a fundamental point of view, these new templates are useful for preparing nanostructures with very small diameters in order to further explore the effects of the dimensionality on the properties of materials. From a technological point of view, this new generation of templates offers potential developments and improvements in the fabrication of nanodevices.

In this paper, we first describe the synthesis of vertically aligned PPy nanotube arrays, obtained by electropolymerization into nanopores of supported polymeric track-etched templates. As the electronic and optical properties of conductive polymers are inherently related to their local structure, different synthesis conditions (template pore size, electrosynthesis temperature and potential) to prepare nanoshaped PPy were investigated. The study of the electronic structure and spectroelectrochemical properties of conductive polymer nanotube brushes is then presented. The doping level, the conjugation length and the electronic structure of PPy in the nanotubes were determined by X-ray photoelectron (XPS), Raman and UV–Vis–NIR spectroscopies and compared to PPy in the bulk form (PPy films). For the first time, thanks to the new PC templates supported on ITO glass, we were also able to investigate the optical properties of conductive polymer nanotubes. We report here on the study of the electroactivity and electrochromic changes occurring in PPy nanotubes, performed by UV–Vis spectroelectrochemistry.

2. Experimental

2.1. PPy films and nanotubes electrosynthesis

$LiClO_4$ (Janssen Chemica) was used without any prior purification. Pyrrole (99%, Acros) was purified immediately before use by passing it through a micro-column constructed from a Pasteur pipet, glass wool and activated alumina. Milli-Q water (18 $M\Omega\,cm^{-1}$) was used to prepare all aqueous solutions.

Two kinds of conductive substrates were used: Indium–Tin Oxide (ITO, Sheet resistance, $Rs = 10\ \Omega$) coated glass and gold-coated silicon wafers. The gold substrates were prepared by successive vacuum evaporation of 15 nm of Ti and 350 nm of Au on the Si wafers. Titanium enhances the adhesion between gold and the silicon substrate. Prior to their use, the gold coated wafers and ITO coated glasses were cleaned by UV-Ozone.

PPy films (thickness of 1–2 μm) were electrochemically synthesized directly on the conducting substrates. PPy nanotubes were prepared by electrosynthesis within the pores of PC supported templates with pore sizes ranging from 20 to 100 nm, pore density of 2×10^8 pores/cm^2 and thickness of 350 and 1200 nm. These new nanoporous templates, supported on ITO-coated glass or gold-coated silicon wafers, were prepared by a track-etching method described elsewhere [16].

Pyrrole electropolymerization was performed in a conventional one-compartment cell, with a Pt counter-electrode and an Ag/AgCl reference electrode. The gold or ITO acted as working electrode. Electrosyntheses were performed at 20 °C from a 0.1 M pyrrole/0.1 M $LiClO_4$ aqueous solution and at 0 °C and −10 °C from 0.1 M pyrrole/0.1 M $LiClO_4$ dissolved in a mixture of methanol and water (1:1, v/v). The electrolyte solutions were deoxygenated with N_2 prior to electrosynthesis. PPy films and nanotubes were grown potentiostatically at +0.65 or +0.8 V using an EG&G Princeton Research Model 273A potentiostat/galvanostat. When the first nanotubes emerge at the top surface of the template, a sudden increase of the current is observed. The growth of PPy nanotubes was stopped at that point to avoid the formation of PPy caps or films on the template surface. PPy films and nanotubes were left to relax in the electropolymerization solution at open circuit during 15 min, then carefully rinsed with Milli-Q water and dried under N_2.

2.2. UV–Vis-NIR spectroscopy

UV–Vis–NIR absorption spectra of PPy films and nanotubes grown on ITO coated glass were recorded on a Varian Cary 500 Scan UV–Vis–NIR spectrophotometer. A virgin ITO coated glass was used as baseline.

2.3. UV–Vis spectroelectrochemistry

PPy films and nanotubes grown on ITO coated glass were placed in a quartz cuvette of 1 cm path length, containing a monomer free electrolyte (0.1 M $LiClO_4$) aqueous solution. ITO was acting as working electrode. A platinum wire was used as counter electrode and Ag/AgCl as reference electrode. The UV–Vis spectra were recorded concomitantly with the application of a potential varying from −900 to +500 mV. A virgin ITO coated glass was used to record the baseline. The presented spectra were recorded 5 min after the potential application, when a constant absorbance was reached. UV–Vis–NIR and UV–Vis spectroelectrochemistry were performed on PPy nanotubes brushes after PC dissolution in CH_2Cl_2 in order to avoid interferences arising from the template.

2.4. Raman spectroscopy

Raman spectra of PPy films and nanotubes attached to the surface of gold-coated Si substrates were recorded 24 h after the electrosynthesis using a dispersive Dilor spectrophotometer with an incorporated microscope equipped with a $He–Ne^+$ laser emitting at 632.8 nm. In this case, the PC template was not removed for the analysis of PPy nanostructures and gave no rise to band in the investigated wavenumber range. The fluorescence background was

removed from the spectra. In this work, a polynomial baseline on the fifth order was subtracted from the spectra.

2.5. Electron microscopy

The morphology of the PPy nanostructures was analyzed using a High Resolution FEG Digital Scanning Microscope 982 Gemini from Leo, operating at 1 kV, after dissolution of the PC template.

2.6. X-ray photoelectron spectroscopy (XPS)

XPS data were obtained using a SSI X probe (SSX 100/206) spectrometer from Fisons, equipped with an aluminium anode (10 keV) and a quartz monochromator. Spectra were taken and recorded at a take-off angle of 35° between the plane of the sample surface and the entrance lens of the detector optics. PPy films were analyzed without any prior treatment. PPy nanotubes were analyzed on the gold-coated Si substrate after removing the PC template. All binding energies were referenced to the C1s neutral carbon peak at 284.8 eV. Curve fitting has been done using a Gaussian–Lorentzian (85%–15%) linear combination and a linear background. The linewidths (FWHM) of the peaks were maintained constant for all the components in a particular spectrum.

3. Results and discussion

3.1. Preparation of PPy nanotubes brushes

It is well established that the electrosynthesis conditions of conductive polymers affect their morphology and physical properties [17]. For that reason, PPy/ClO_4 nanotubes were electrochemically synthesized within the pores (different diameters) of supported nanoporous templates under various experimental conditions: different electrosynthesis temperatures (−10, 0 and 20 °C) and two different electrosynthesis potentials (+0.65 and +0.8 V vs. Ag/AgCl). Fig. 1 presents, at one hand, a schematic representation of the main steps of PPy nanotubes electrosynthesis within the nanopores of the supported template and on the other hand, SEM pictures of the supported template surface (Fig. 1a) and of PPy nanotubes tethered to the conductive substrate (Fig. 1b). This last picture was recorded after PC dissolution in dichloromethane (CH_2Cl_2).

The dependence of PPy nanotubes growth rate on pore size, synthesis temperature and electrodeposition potential was investigated. For all the studied electrosynthesis conditions, it appears that the nanotubes growth rate decreases with pore size. At room temperature, the growth rate of PPy nanotubes within supported templates with pore size of 60 nm reaches ±100 nm/s at a working potential of +0.8 V. Due to this high growth rate, the control of the nanotubes length at +0.8 V was difficult. Therefore, in order to prepare PPy nanotubes with well-controlled dimensions and in particular, to avoid the formation of PPy caps or film at the extremities of the tubes, PPy electrodeposition was performed most of the time at +0.65 V. At this electrodeposition potential, the growth rate was drastically reduced (down to 3–4 nm/s for pore size of 60 nm) allowing an easier control of the electropolymerization process. Decreasing the electropolymerization temperature also leads to a decreasing of the nanotubes growth rate. For instance, PPy growth rate at a working potential of +0.65 V within pores of 60 nm in diameter is equal to 1 nm/s.

Each PPy nanotube array was characterized by XPS, Raman and UV–Vis–NIR spectroscopies. For comparison, PPy/ClO_4^- films were also prepared and characterized under similar experimental conditions.

3.2. X-ray photoelectron spectroscopy

XPS is a particularly useful tool for obtaining information on the doping level of electroactive polymers. This method has now been often used to characterize PPy films [18–22] and was once used for the characterization of chemically synthesized PPy nanotubes [15].

Typical N(1s) curve fitted core level spectra of PPy/ClO_4^- films and nanotubes electrosynthesized at room temperature are presented in Fig. 2. Previous XPS studies on PPy have demonstrated that the imine like (=N–), amine like (–NH–) and positively charged nitrogen atoms ($–N^+$) corresponding to any particular intrinsic oxidation state and protonation level of the polymer can be quantitatively differentiated in the curve-fitted N(1s) core-level spectrum. They correspond to peak components with binding energies at about 397.8, 399.9 and above 401 eV, respectively [15,23,24]. Unusual peaks around 406 eV also appear in the core-level N1s spectra of nanotubes and films. According to Skotheim et al. [23], the presence of this peak can be related to the presence of pyrrole oligomers or to shake-up (simultaneous core-electron excitations and π–π* transitions from the highest occupied to the lowest unoccupied valence levels of the conducting polymer). Table 1 summarizes the proportions of the N1s peak components for PPy films and nanotubes (with two different outside diameters: 85 and 35 nm) electrosynthesized in different conditions.

Eaves et al. [20] have attempted to quantitatively associate the fraction of the N1s spectrum arising from high binding energy components ($[N^+]$/[N] ratio) to the Cl/N ratio. Assuming that all oxidized N bear a unit positive charge, a good correlation was found for PPy samples synthesized in different conditions or subjected to different chemical treatment [25]. As in the case of PPy nanotubes samples, the XPS analyzed area is composed of less than 10% of nanotubes (the remaining 90% being the gold substrate), chlorine content due to the presence of ClO_4^- doping anions was too low to be detected. Consequently, the

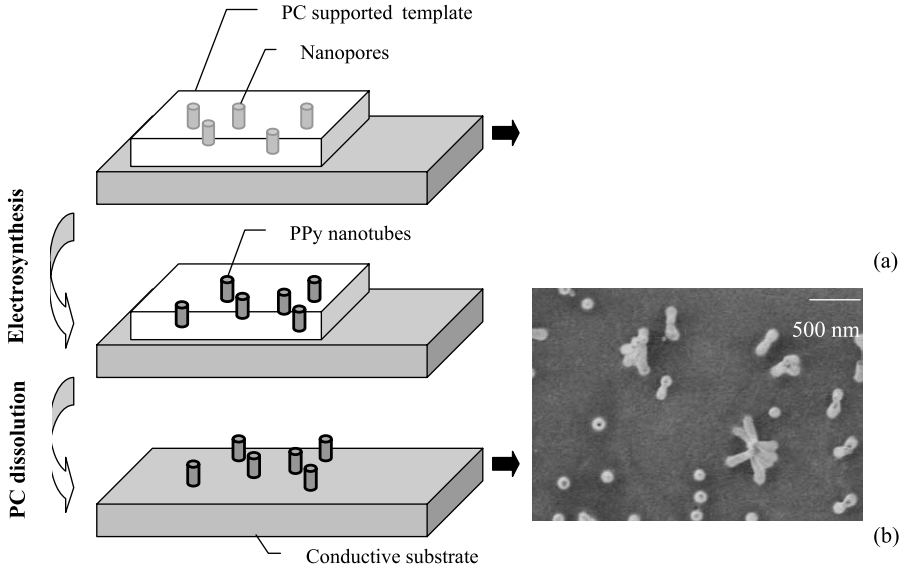

Fig. 1. Sketch of the PPy template synthesis in new PC supported templates and the corresponding SEM images of (a) the template surface and (b) PPy nanotubes tethered to the conductive substrate (image recorded after template dissolution).

doping level in PPy nanotubes could not be estimated by the Cl/N ratio. So, we did it by the $[N^+]/[N]$ ratio. Results presented in Table 1 show that in all the studied synthesis conditions, this ratio is lower for PPy nanotubes than for the corresponding film. Moreover, it appears that the doping level is affected by the nanotubes diameter and by the electropolymerization potential and temperature. For samples electrosynthesized at +0.65 V (conditions A to C), large differences in the doping level can be noticed between PPy films ($25.5\% < ([N^+]/[N] < 28.8\%$) and PPy nanotubes ($11.4\% < ([N^+]/[N] < 13.3\%$, for the 85 nm diameter nanotubes and only $8.0\% < ([N^+]/[N] < 10.8\%$ for the 35 nm ones). The lowest doping levels were obtained for samples electrosynthesized at the lowest studied temperature, −10 °C. The fact that lower doping levels were reached for nanotubes than for films could be linked to the limited diffusion of the counter-anions when PPy is synthesized in confined media (nanopores). Increasing the electropolymerization potential up to +0.8 V (conditions D) significantly enhances the doping levels of PPy nanotubes (up to ca. 25%) but they still remain lower than the doping level of the corresponding PPy film (close to 30%). In a similar way, a post-treatment consisting in the application of an oxidation potential in a monomer free

Table 1
N1s peaks proportions extracted from the XPS spectra of PPy/ClO_4^- films and nanotubes prepared in various electrodeposition conditions

Sample	N1s component proportions (%)		
	397.8 eV –N=	399.9 eV –NH–	>401 eV $–N^+$ (doping level)
Conditions A			
Film	2.8	68.4	28.8
Nanotubes $\Phi = 85$ nm	7.8	79.5	12.7
Nanotubes $\Phi = 35$ nm	17.1	72.1	10.8
Conditions B			
Film	0	72.5	27.5
Nanotubes $\Phi = 85$ nm	12.0	74.7	13.3
Nanotubes $\Phi = 35$ nm	27.0	64.5	8.5
Conditions C			
Film	3.6	74.5	25.5
Nanotubes $\Phi = 85$ nm	11.7	76.9	11.4
Nanotubes $\Phi = 35$ nm	17.4	74.6	8.0
Conditions D			
Film	5.1	65.4	29.5
Nanotubes $\Phi = 85$ nm	3.2	71.2	25.6
Nanotubes $\Phi = 35$ nm	8.4	66.5	25.1

Conditions A: Electrosynthesis at +0.65 V vs. Ag/AgCl and at 20 °C from an aqueous solution 0.1 M pyrrole/0.1 M $LiClO_4$, at +0.65 V vs. Ag/AgCl. Conditions B and C: Electrosynthesis at +0.65 V vs Ag/AgCl from a 0.1 M pyrrole/0.1 M $LiClO_4$ solution in H_2O/methanol (1:1, v/v), at 0 °C and −10 °C, respectively. Conditions D: Electrosynthesis at +0.8 V vs. Ag/AgCl and at 20 °C from an aqueous solution 0.1 M pyrrole/0.1 M $LiClO_4$.

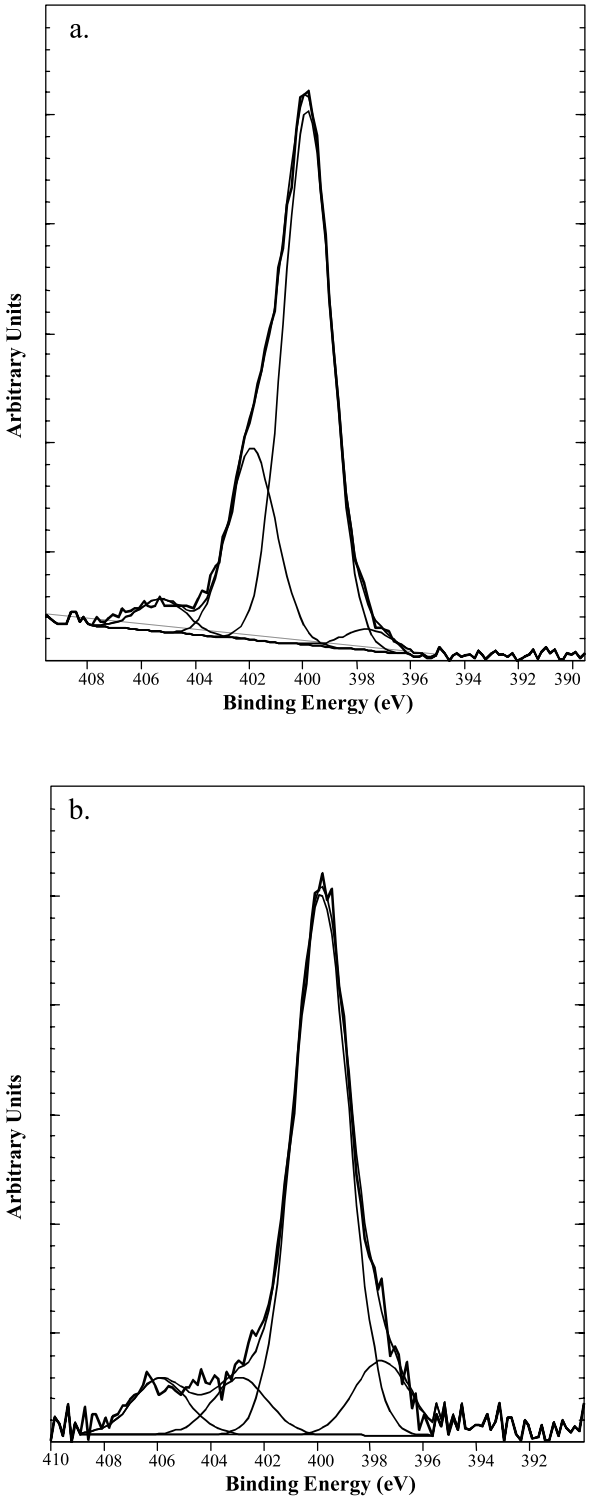

Fig. 2. Core-level N1s spectra of (a) PPy film and (b) nanotubes electrosynthesized at 20 °C and at +0.65 V.

solution (0.1 M $LiClO_4$) to PPy nanotubes electrosynthesized at +0.65 V allows to increase their doping level. The post-treatment was performed on nanotubes embedded within the PC template. After application of a potential of +0.5 V during 30 min, the doping level of PPy nanotubes with outside diameter of 85 and 25 nm reaches 22 and 18%, respectively. Longer oxidation post-treatment did not lead to a further increase of the doping level.

3.3. Raman spectroscopy

It has already been demonstrated that vibrational spectroscopies, in particular Raman spectroscopy, is a powerful tool for elucidating the molecular and electronic structure of conducting polymer [26,27]. In this work, Raman analyses were conducted on PPy films and PPy nanotubes electrochemically synthesized in various conditions onto gold-coated silicon wafers. The low rugosity (Rms < 30 Å) of these gold-coated substrates allows us to get well-resolved spectra characteristic of polypyrrole for both films and nanotubes. Typical Raman spectra of PPy/ClO_4^- film and nanotubes of different outside diameters are shown in Fig. 3. The assignment of the bands according to Furukawa et al. [25] is provided in Table 2. One can notice that the ring deformation mode and the symmetric CH-in plane bending modes are split due to contributions from the radical cations (polarons) and dications (bipolarons): peaks at 934 and 1086 cm^{-1} are associated with the bipolaron structure and those at 968 and 1055 cm^{-1} are associated to the polaron structure.

In previous studies, the band ratio between the intensity of a band sensitive to the oxidation state of the polymer (i.e., 1595 cm^{-1}) and the intensity of the skeletal band (i.e., 1500 cm^{-1}) was used to get a qualitative measurement of the conjugation length (L) [4,14]. This ratio was calculated for different PPy samples and the results are reported in Table 3. Taking into account the experimental errors due to the poor resolution of the 1500 cm^{-1} band, a continuous increase of the 1595/1500 intensity ratio is observed when going from PPy films to narrow PPy nanotubes (Table 3). This increase of the intensity of the C=C stretching band vs. the intensity of the skeletal band means that the polarizability of the system is higher for the narrower PPy nanotubes or, in other words, that the relative conjugation length is higher in PPy nanotubes (in particular, in narrow PPy nanotubes) than in PPy films. These results are in perfect agreement with those reported earlier by Martin et al. who determined the relative conjugation length by polarized infrared absorption spectroscopy (PIRAS) [15].

Different ratios [Eqs. (1–3)] between the intensities of the bands relative to bipolarons (934 and 1086 cm^{-1}) and polarons (968 and 1055 cm^{-1}) can be used to estimate the [bipolarons]/[polarons] ratio [28,29].

$$R_1 = \frac{I(934\ \mathrm{cm}^{-1})}{I(968\ \mathrm{cm}^{-1})} \quad (1)$$

$$R_2 = \frac{I(1086\ \mathrm{cm}^{-1})}{I(1055\ \mathrm{cm}^{-1})} \quad (2)$$

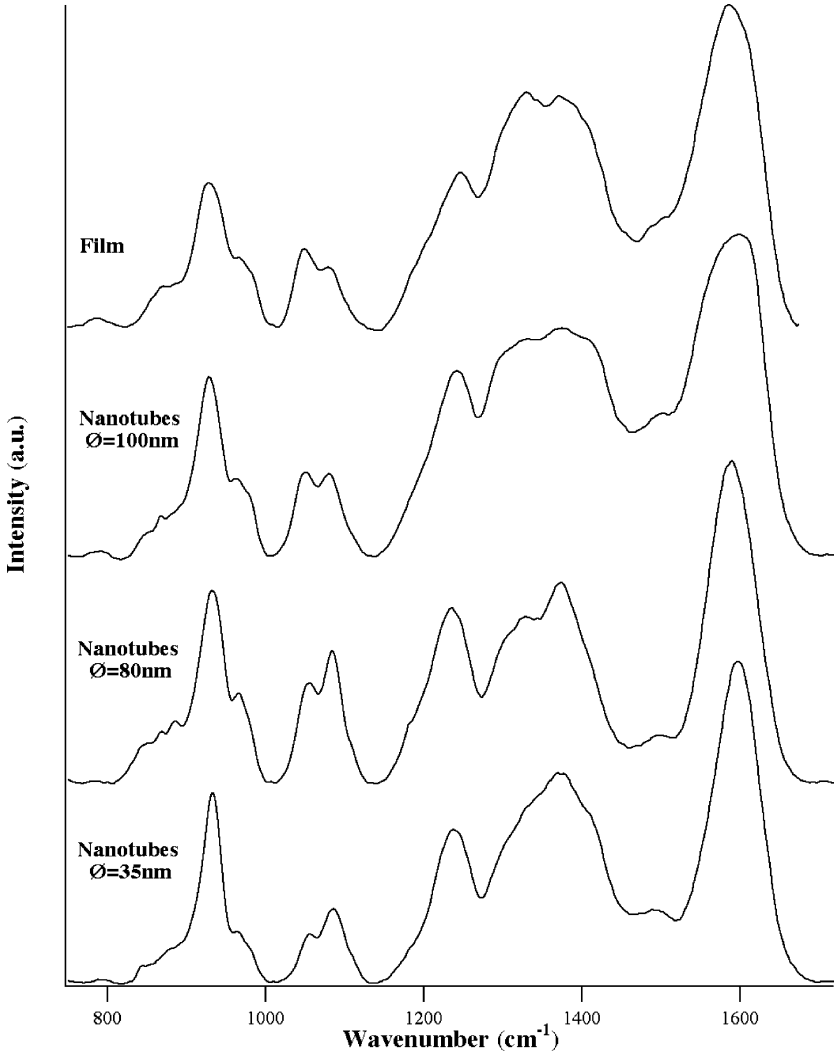

Fig. 3. Raman spectra of PPy films and PPy nanotubes with different outside diameters.

$$R_3 = \frac{I(934\ \mathrm{cm}^{-1}) + I(1086\ \mathrm{cm}^{-1})}{I(968\ \mathrm{cm}^{-1}) + I(1055\ \mathrm{cm}^{-1})} \quad (3)$$

These ratios, R_1, R_2 and R_3 are reported for different PPy films and nanotubes in Table 3. All these ratios were found to be significantly higher for nanotubes than for films. Moreover, they increase when the nanotubes diameter decreases. Whatever the electrosynthesis conditions, the highest bipolaron content was always found for the narrowest PPy nanotubes.

3.4. UV–Vis–NIR spectroscopy and UV–Vis spectroelectrochemistry

Finally, the electronic structure and the spectroelectrochemical properties of PPy within the nanostructures were carefully studied by UV–Vis–NIR spectroscopy and UV–Vis

Table 2
Assignments of PPy Raman bands following Furukawa et al. [23]

Band position	Assignment
934 cm^{-1}	Ring deformation associated with dication
968 cm^{-1}	Ring deformation associated with radical cation
1050 cm^{-1}	Symmetrical C–H in plane bending associated with radical cation
1080 cm^{-1}	Symmetrical C–H in plane bending associated with dication
1255 cm^{-1}	Antisymmetrical C–H in plane bending
1380 cm^{-1}	Antisymmetrical C–N stretching
1500 cm^{-1}	Skeletal band
1595 cm^{-1}	C=C stretching

Table 3
Raman bands intensity ratios, characterizing the [Bipolarons]/[Polarons] concentration (R_1, R_2 and R_3) and Raman bands intensity ratio characteristic of the relative conjugation length (L) for PPy films and nanotubes prepared in various electrosynthesis conditions

Sample	R_1	R_2	R_3	L
Conditions A				
Film	0.5	0.8	1.4	1.2
Nanotubes $\Phi=85$ nm	2.7	1.2	1.9	4.9
Nanotubes $\Phi=35$ nm	3.0	1.3	2.1	5.6
Conditions B				
Film	1.3	0.5	1.5	2.2
Nanotubes $\Phi=85$ nm	2.5	1.1	1.8	3.4
Nanotubes $\Phi=35$ nm	2.6	1.5	2.0	3.3
Conditions C				
Film	2.4	0.5	1.4	1.6
Nanotubes $\Phi=85$ nm	2.5	1.3	1.9	3.3
Nanotubes $\Phi=35$ nm	2.8	1.3	2.0	6.5
Conditions D				
Film	2.4	0.5	1.2	1.9
Nanotubes $\Phi=85$ nm	2.4	0.9	1.5	2.9
Nanotubes $\Phi=35$ nm	3.6	1.1	2.3	2.5

Conditions A: Electrosynthesis at +0.65 V vs. Ag/AgCl and at 20 °C from an aqueous solution 0.1 M pyrrole/0.1 M $LiClO_4$, at +0.65 V vs. Ag/AgCl. Conditions B and C: Electrosynthesis at +0.65 V vs. Ag/AgCl from a 0.1 M pyrrole/0.1 M $LiClO_4$ solution in H_2O/methanol (1:1, v/v), at 0 °C and −10 °C, respectively. Conditions D: Electrosynthesis at +0.8 V vs. Ag/AgCl and at 20 °C from an aqueous solution 0.1 M pyrrole/0.1 M $LiClO_4$.

spectroelectrochemistry. UV–Vis–NIR absorption spectra of PPy films and different PPy nanotubes tethered to ITO glass substrates were recorded. Some typical spectra are displayed on Fig. 4. All of them are characteristics of doped PPy and are dominated by a broad absorption band at low energy, around 1 eV. The bandwidth and maximum location of this peak depend on the considered sample. This first electronic transition, assigned to the transition between the valence band (VB) and the bonding bipolaronic band [30], shifts from 1.16 eV for PPy films to a lower value, 1.05 eV, for PPy nanotubes. Moreover, the bandwidth is significantly reduced for PPy nanotubes. Two other absorption bands located at 2.84 and 3.3 eV for films, 2.48 and 3.81 eV for large PPy nanotubes ($\Phi=85$ nm), and 2.21 and 3.89 eV for narrow PPy nanotubes ($\Phi=35$ nm) also appear in the spectra. In the case of PPy films, these two bands can be assigned to the electronic transition between the VB and the antibonding bipolaronic band and to the π–π* transition, respectively [30]. The attribution of the electronic transitions is however, more complicated for PPy nanostructures. The absorptions at 3.81 and 3.89 eV seem indeed too high to be attributed to the π–π* transition. In order to properly identify the electronic transitions and to check the elctroactivity of the polymer, an UV–Vis spectroelectrochemistry study was carried out on PPy nanotubes and on PPy films, for comparison. PPy samples (nanotubes and films) were subjected to a potential sweep from −900 to +500 mV. Fig. 5a presents the evolution of the PPy film

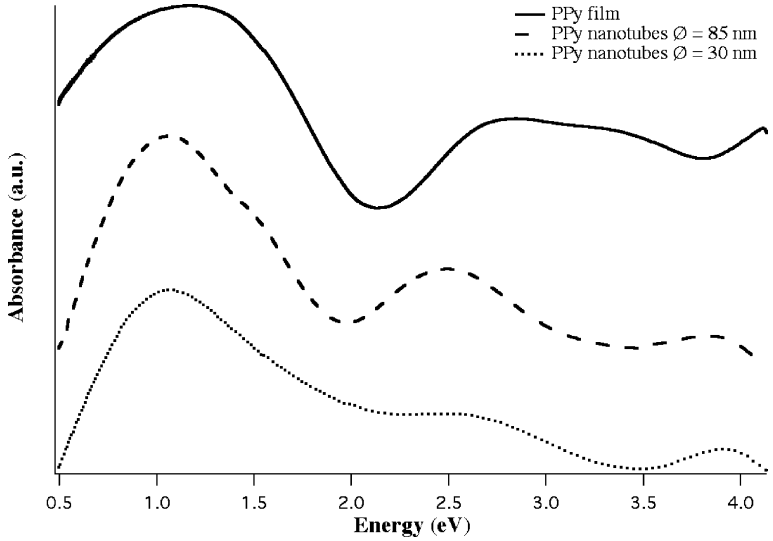

Fig. 4. UV–Vis–NIR spectra of as-synthesized (a) PPy film, (b) PPy nanotubes with outside diameter of 85 nm and (c) PPy nanotubes with outside diameter of 35 nm.

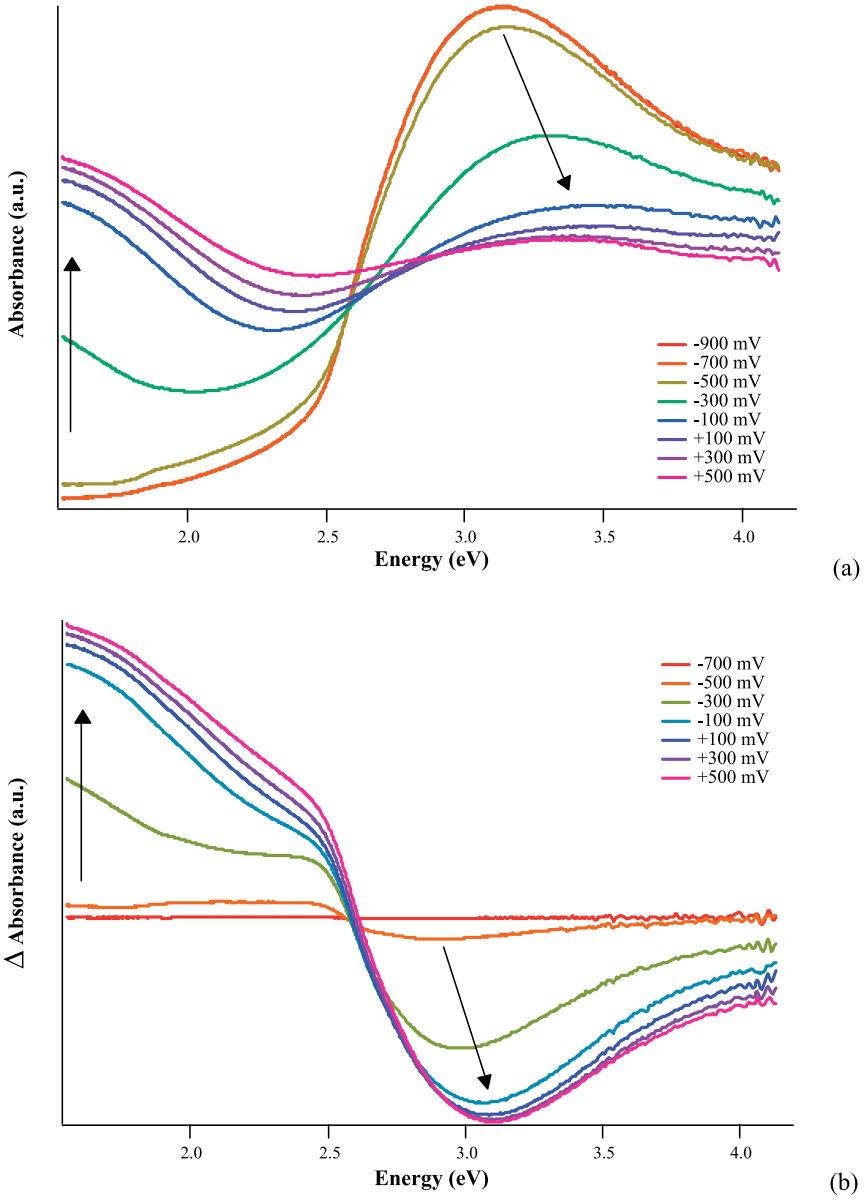

Fig. 5. (a) UV–Vis spectra of PPy films recorded during a potential sweep from −900 to +500 mV, (b) Different UV–Vis spectra of the PPy film during the same potential sweep.

absorption upon oxidation and reduction. In good agreement with previous studies, the reduced PPy film shows a maximum of absorbance at 3.14 eV related to the π–π* transition of neutral PPy. Upon oxidation, this maximum shifts to higher energy and decreases in intensity. Simultaneously, a new absorption band appears at lower energy. In the fully oxidized sample, the spectrum is dominated by this transition around 1.55 eV.

The spectroelectrochemical data obtained for PPy nanotubes were significantly different than those obtained for PPy films. Fig. 6a presents the spectra of PPy nanotubes (Φ = 85 nm) recorded during a potential sweep from −900 to +500 mV. The spectra recorded at −900 mV of nanotubes with diameters of 85 and 35 nm (not shown) are dominated by one peak located at 2.73 and 2.99 eV, respectively. A shoulder at higher energy, around 3.8 eV, already observed in the UV–Vis–NIR spectra recorded under ambient atmosphere (Fig. 4), is also detected. The different spectra presented in Figs. 5b and 6b were calculated by subtracting the first spectrum recorded at −900 mV (reference of the sample) from all the consecutive spectra. By this way, only the electronic transitions sensitive to the oxidation or reduction of PPy appear in the difference spectra, the electronic transitions not affected by the redox process being eliminated. For PPy nanotubes, the disappearance of the high-energy absorption shoulder (ca. 3.8 eV) demonstrates that this band is not sensitive to the applied potential and can thus not be attributed to the π–π*

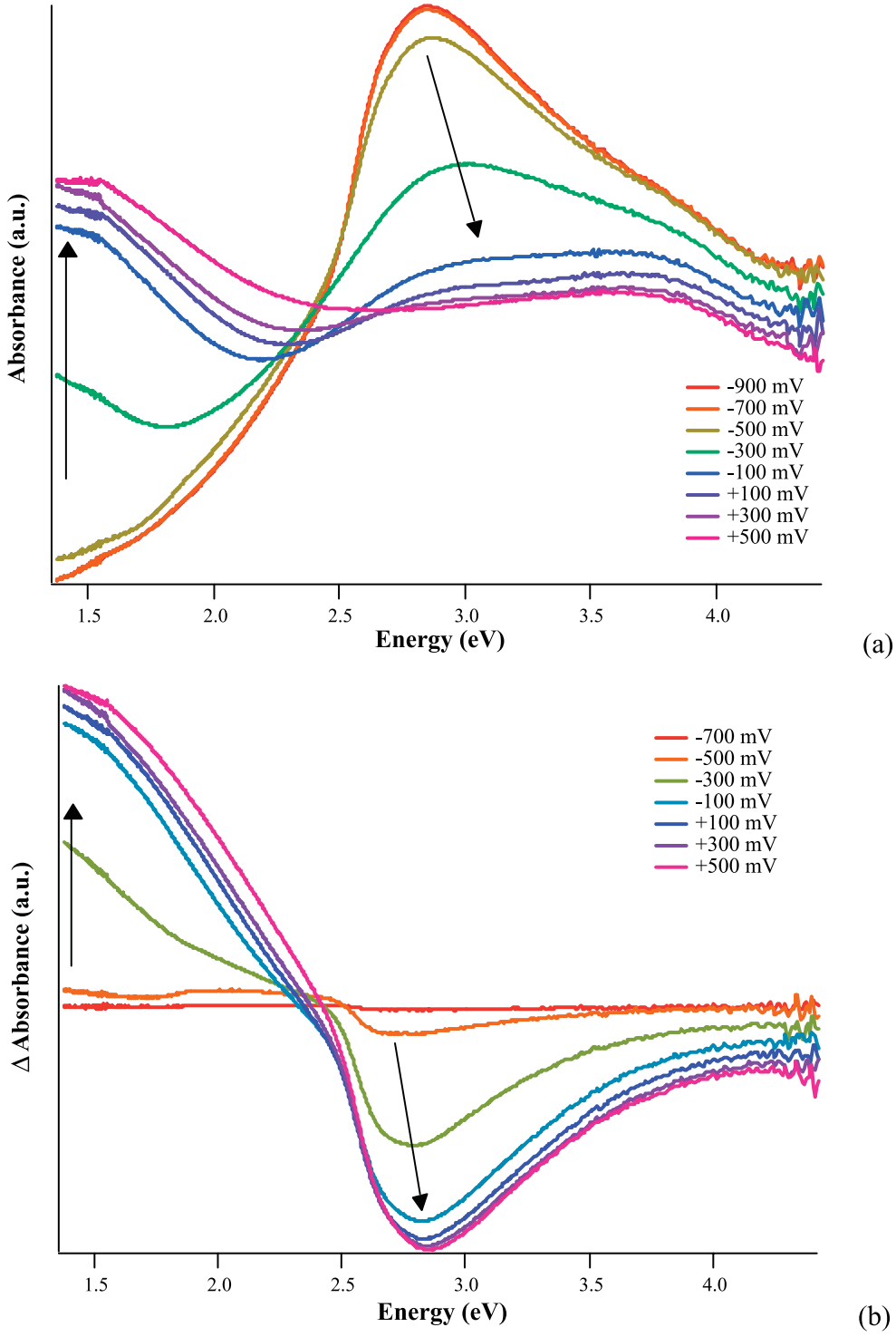

Fig. 6. (a) UV–Vis spectra of PPy nanotubes with outside diameter of 85 nm recorded during a potential sweep from −900 to +500 mV, (b) Different UV–Vis spectra of the PPy nanotubes during the same potential sweep.

transition of the conducting polymer. This band appears only for PPy nanotubes and its intensity is higher for the narrowest nanostructures. It could be related to the presence of pyrrole oligomers confined into the nanostructures [31]. The absorption bands at 2.73 and 2.99 eV observed in the spectra recorded at −900 mV of PPy nanotubes presenting diameters of 85 and 35 nm, respectively, can, therefore, be attributed to the interband π–π* transition. During PPy nanotubes oxidation, this absorbtion band decreases in intensity and shifts towards lower energy. At increasing oxidation levels, a shoulder at 2.38 eV and a broad absorption band below 1.38 eV appear in the spectrum.

These bands are attributed to the transition between the VB and the anti-bonding bipolaronic band and to the transition between the VB and the bonding bipolaronic band, respectively. The redox switching of PPy was not fully reversible at the first potential cycle, but the electroactivity then remained stable during the next cycles.

Additional information can be extracted from the UV–Vis spectroelectrochemical spectra of PPy films and nanotubes. The spectra can indeed be decomposed assuming three components: neutral (N), polaronic (P) and bipolaronic (B). Applying the Lambert–Beer law, the resulting absorbance, at a given potential (V), is then considered to be a linear combination of these three components (Eq. [4]).

$$\text{Abs}\,(\lambda, V) = k_1\text{N}(\lambda, V) + k_2\text{P}(\lambda, V) + k_3\text{B}(\lambda, V) \quad (4)$$

Zotti et al. [32] used this technique to determine the evolution of the polaron proportion in PPy and PANi films. More recently, Rapta et al. [33] determined the quantitative time dependences of neutral, polaron and bipolaron species in PPy films during redox cycling using data from in-situ ESR/UV–Vis experiments. Thanks to cyclic voltammetry and EPR data, the superimposed UV–Vis spectra were separated into components corresponding to the individual redox states using a least-squares method. Similarly, Aubert et al. [29] compared the optical behavior of different pyrrole copolymers.

Using the same mathematical peak separation procedure [34], our PPy films and nanotubes UV–Vis spectra were decomposed into their three components. The used model assumed that: (1) at the starting potential of −900 mV, no charge carriers remain and that only the neutral component contributes to the absorbance; (2) at the switching potential of +500 mV, only bipolarons contribute to the absorbance. This is only an approximation because at +500 mV the dominant species are indeed bipolarons but some polarons can still remain. The error induced by this second condition is however, minimized, as the polaron signal measured for PPy films by in-situ ESR spectroelectrochemistry decreases to zero around this potential [33].

The evolution of the contributions (k_1, k_2, k_3) of the different components to the absorption spectra for PPy films and nanotubes during redox cycling is presented on Fig. 7. These contributions cannot be directly related to the molar concentrations of the different species, their respective molar absorbance coefficients being unknown. They, however, give us qualitative information on the evolution of the different species proportions during oxidation and reduction of PPy in the different form (films or nanotubes). Upon oxidation (going from −900 to +500 mV), at low potentials the neutral species are dominant for films and nanotubes. With increasing potential, polaron proportion increases and reaches a maximum at −300 mV for films and at −100 mV for nanotubes. At higher potentials, the polaron proportion decreases indicating their recombination into bipolarons. During reduction (going from +500 to −900 mV), bipolarons progressively disappear and the polaron proportion increases up to a maximum around −300 mV. For PPy film, the bipolarons proportion reaches nearly zero at −700 mV, whereas for PPy nanotubes, a significant bipolaron contribution is still observed at −900 mV. Moreover, some polarons are still present in PPy films and nanotubes at potentials as low as −900 mV. Further reduction of the samples at an applied potential of −1.1 V for 2 h does not allow to eliminate all these charge carriers. This phenomenon could be explained as folllows: during oxidation of the polymer, the layers near the electrode surface are first transformed into the oxidative conductive state which enables further oxidation of the upper layers, until the fully oxidized state is reached. During reduction the polymer layers near the electrode are the first transformed into the neutral insulating form of the polymer and the further reduction of more distant layers is partially inhibited by these passivated layers. Consequently, polarons and bipolarons can remain in PPy film and nanotubes even at low applied potentials.

4. Conclusions

Homemade supported PC templates were used to prepare vertically aligned PPy nanotube arrays. The influence of different electrosynthesis parameters on the structure and properties of PPy nanotubes was studied using different spectroscopies. Under similar electrosynthesis conditions, the doping level estimated by XPS was always significantly lower for PPy nanotubes than for films. Moreover, the doping level of PPy nanotubes clearly depends on the electrosynthesis conditions. As revealed by Raman spectroscopy, whatever the electrosynthesis conditions, PPy nanotubes present higher relative conjugation length and a higher proportion of bipolarons than the corresponding film. Finally, as observed by UV–Vis–NIR spectroscopy and UV–Vis spectroelectrochemistry, the electronic structure of nano-shaped PPy presents some interesting characteristics. First, the π–π* transition occurs at significantly lower energy for PPy nanotubes than for PPy films. Secondly, as PPy films, PPy nanotubes are electroactive and can thus be switched between a conductive and insulating state.

From a fundamental point of view, the different results reported in this paper contribute to the explanation of the genesis of the particular electrical behavior of PPy nanotubes that others and we have previously reported [5,6,12–15]. Indeed, the enhancement of the room-temperature electrical conductivity observed for PPy nanotubes can be, atleast partially, attributed to the higher relative conjugation length, the higher bipolaron content and the lower energy π–π* transition of the polymer in these nanostructures. From a technological point of view, the process developed in this work offers the possibility to prepare conjugated

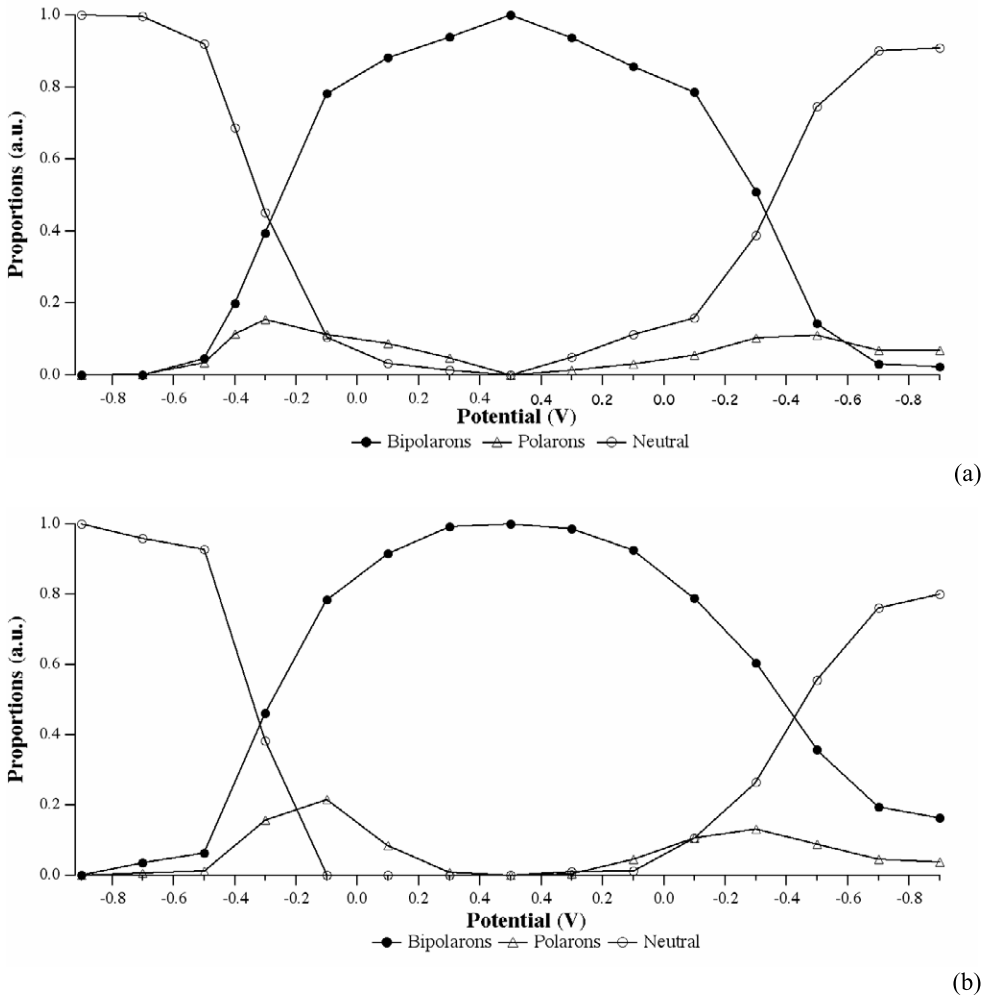

Fig. 7. Evolution of the contributions of the different components to the UV–Vis spectra: neutral, polaron and bipolaron contributions during a redox cycle from −900 to +500 mV for (a) PPy film and (b) PPy nanotubes with outside diameter of 35 nm.

polymers with an engineered nanoshape of various aspect ratios directly tethered to the device surface. This point is very interesting for the development of different applications based on nanotubes or nanowires as the process is not limited to the production of polymeric nanomaterials but could also be used for the preparation of metallic [35] or metal oxides nanowires.

Acknowledgements

S. D-C thanks the Belgian National Fund for Scientific Research (F.N.R.S.) for her Research Associate position. L. D-D is a fellow of the "Fonds pour la formation à la recherche dans l'industrie et dans l'agriculture" (FRIA, Belgium). The authors wish to thank Dr J-L. Duvail for helpful discussions. This work was partially supported by the 'Ministère de la Région Wallonne, Direction Générale des Technologies, de la Recherche et de l'Energie' (Convention n° 9914152) and by the European Community (Convention n° GRD1-1999–10248).

References

[1] Ozin GA. Adv Mater 1992;4:612–49.
[2] Martin CR. Science 1994;266:1961–6.
[3] Schönenberger C, van der Zande BMI, Fokkink LGJ, Henny M, Schmid C, Krüger M, et al. J Phys Chem 1997;101:5497–505.
[4] Demoustier-Champagne S, Stavaux PY. Chem Mater 1999;11:829–34.
[5] Delvaux M, Duchet J, Stavaux PY, Legras R, Demoustier-Champagne S. Synth Met 2000;113:275–80.
[6] Martin CR. Chem Mater 1996;8:1739–46.
[7] Hulteen JC, Martin CR. J Mater Chem 1997;7(7):1075–87.
[8] Martin CR, Van Dyke LS, Cai Z, Liang W. J Am Chem Soc 1990;112:8976–7.
[9] Mansouri J, Burford RP. J Membr Sci 1994;87:23–34.
[10] Mansouri J, Burford RP. J Mater Sci 1994;29:2500–6.
[11] Granström M, Carlberg JC, Inganäs O. Polymer 1995;36:3191–6.
[12] Granström M, Inganäs O. Polymer 1995;36:2867–72.
[13] Cai Z, Martin CR. J Am Chem Soc 1989;111:4138–9.
[14] Duchet J, Legras R, Demoustier-Champagne S. Synth Met 1998;98:113–22.
[15] Menon VP, Lei J, Martin CR. Chem Mater 1996;8:2382–90.
[16] Dauginet-De Pra L, Ferain E, Legras R, Demoustier-Champagne S. Nucl Instrum Methods B 2002;196:81–8.

[17] Rodriguez J, Grande H-J, Otero TF. In: Nalwa HS, editor. Handbook of organic conductive molecules and polymers, 2. Chichester, England: Wiley; 1997. p. 415–68. Chapter 10.
[18] Kang ET, Neoh KG, Tan KL. Adv Polym Sci 1993;106:135–90.
[19] Pfluger P, Street GB. J Chem Phys 1984;80(1):544–53.
[20] Eaves JG, Munro HS, Parker D. Polym Commun 1987;28:38–40.
[21] Malitesta C, Morea G, Sabbatini L, Zambonin PG. In: Sabbatini L, Zambonin PG, editors. Surface characterization of advanced polymers. Weinheim, Germany: VCH Pub Inc.; 1993. p. 181–219.
[22] Salaneck WR, Erlandsson R, Prejza J, Lundström I, Inganäs O. Synth Met 1983;5:125–39.
[23] Skotheim TA, Florit MI, Melo A, O'Grady WE. Phys Rev B 1984; 30(8):4846–9.
[24] Kim DY, Lee JY, Kim CY, Kang ET, Tan KL. Synth Met 1995;72: 243–8.
[25] Kang ET, Neoh KG, Ong YK. Synth Met 1990;39:69–80.
[26] Furukawa Y, Tazawa S, Fujii Y, Harada I. Synth Met 1988;24: 329–41.
[27] Gussoni M, Castiglioni C, Zerbi G. In: Clark RJH, Hester RE, editors. Spectroscopy of advanced materials. Chichester: Wiley; 1991. p. 251–353.
[28] Liu YC, Hwang BJ. Synth Met 2000;113:203–7.
[29] Mikat J. Synth Met 2001;119:649–50.
[30] Brédas JL, Scott JC, Yakushi K, Street GB. Phys. Rev. B 1984;30: 1023–5.
[31] Fermin DJ, Scharifker BRJ. Electroanal Chem 1993;357:273–87.
[32] Zotti G, Schiavon G. Synth Met 1989;30:151–8.
[33] Rapta P, Neudeck A, Petr A, Dunsch L. J Chem Soc, Faraday Trans 1998;94:3625–30.
[34] Aubert PH, Neudeck A, Dunsch L, Audebert P, Capdevielle P, Maumy M. J Electroanal Chem 1999;470:77–88.
[35] Vila L, Vincent P, Dauginet-DePra L, Pirio G, Minoux E, Gangloff L, et al. Nano Lett. 2004;4(3):521–4.